Effects of permanent magnet arrangements and antenna locations on the generation of multicusp electron cyclotron resonance plasma

Takashi Namura
Kyoto Research Laboratory, Matsushita Electronics Corporation, Kyoto 601, Japan

Ichio Arikata
Himeji Institute of Technology, Syosha, Himeji 671-22, Japan

Osamu Fukumasa
Department of Electrical Engineering, Yamaguchi University, Ube 755, Japan

Makoto Kubo and Ryohei Itatani
Department of Electronics, Kyoto University, Kyoto 606, Japan

(Received September 3 1991; accepted for publication October 6 1991)

A comparative study on the generation of 2.45-GHz multicusp electron cyclotron resonance (ECR) plasma is performed. Looped cusp structures such as the ring-cusp give a low-power and low-pressure ignition, and vice versa, indicating an importance to keep the electron trajetory of gradient-B drift motion inside the chamber even in the case of ECR plasmas. The importance of the antenna location in such multicusp fields is elucidated by comparison in two cases of the axial antenna located in the weak magnetic field region, generating a hydrogen plasma of limited density ($n_e < 7.4\times10^{10}$ cm^{-3}), and a radial antenna located in the strong magnetic field region, generating an overdense plasma ($n_e \sim 2\times10^{11}$ cm^{-3}).

I. INTRODUCTION

The electron cyclotron resonance (ECR) discharge[1] using a microwave provides several merits in connection with applications: It realizes a selective and localized heating of electrons at the resonance zone, and a good confinement of electrons in case of proper magnetic configurations. Additionally, the microwave usage arrows a small and simple launching system of an electrodeless structure. Many studies on the ECR were carried out so far in the field of fusion research plasmas,[2,3] highly charged ion source plasmas,[4,5] and surface processing plasmas.[6–8] Historically, those ECR plasmas are generated in large magnetic volumes which must be paid in terms of electrical consumption in the coils, whereas small ECR plasmas are often achievable with permanent magnets.[9] To improve the power efficiency, however, the use of a permanent magnet also for the large volume plasma is favorable. The permanent magnets surrounding a discharge volume from a multicusp (multipole) field whose intensity is only significant near the chamber wall, in contrast to the large magnetic volume excited by solenoidal coils[4,6,7] or its combination with permanent magnets.[5,8,10] Moreover, if a proper magnet arrangement is used, one obtains a very weak magnetic volume inside. This type of magnetic configuration provides additional merits of sustaining a magnetohydrodynamically stable nonmagnetized and uniform plasma, as proved by the numerous studies on the multicusp dc plasma[11–19] or externally excited multicusp plasma.[20–24] These properties are desirable especially in the field of surface processing for microelectronics.

In the recent years, several attempts to develop such multicusp ECR devices and its application have been carried out with various magnet arrangements and microwave launching systems. The first efforts to apply a multicusp ECR device to the surface processing were performed by Asmussen and co-workers,[25–32] who used a line-cusp magnet and microwave cavity to produce a plasma in a disk-shaped volume. More recently, Pichot and co-workers used a rod antenna array just along the line-shaped ECR zone of a line-cusp magnet.[33,34] Kretschmer used a horn-shaped waveguide and a ring-cusp magnet to produce a plasma of 30 cmϕ.[35] There are similar efforts in the other fields of application. Goede used a high-Q resonance cavity of 30 cm ϕ with line-cusp or ring-cusp magnets and microwave feeding through a rectangular slot in his study on the space propulsion application.[36] We have also examined some different magnet arrangements and antenna locations in our early studies on the volume production of positive and negative hydrogen ions,[37–41] where preliminary results have demonstrated the efficient ignition of ring-cusp device,[39,40] and the generation of an overdense plasma by using a proper antenna location.[41]

While various types of multicusp ECR devices are working, the discharge process is very different from the historical ECR on the following points: (a) The whole ECR zone is located close to the chamber wall, and the electron diffusion length along the magnetic lines of force is short. (b) Electron gyromotion is complicated due to the large gradient, divergence, and curvature of the magnetic field. (c) Microwave power deposition is not easily described by the plasma wave theory in uniform or small gradient magnetic field[42,43] because the scale length of the magnetic field is shorter than both the vacuum wavelength of the microwave and the size of discharge space. It is clear that the selection of magnet arrangement and microwave launching system has a great importance on the performance of multicusp ECR device. However, there is no systematic work on this point, and the guiding principle to design a multicusp ECR device is still not established.

 0034-6748/92/010021-10$02.00

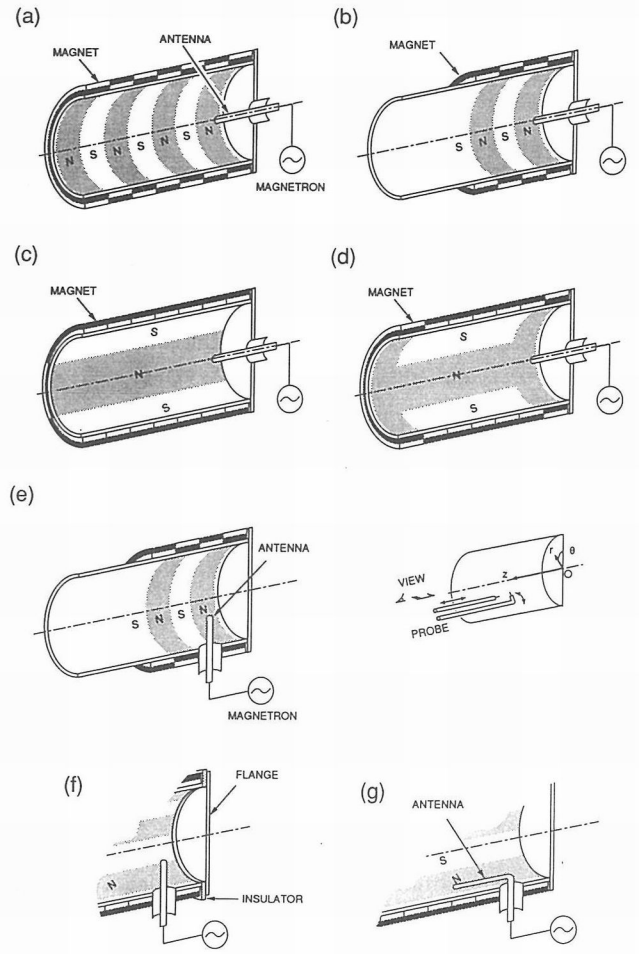

FIG. 1. Magnet arrangements and antenna locations of multicusp ECR devices. The multicusp structures are (a) seven-pole ring-cusp, (b), (e) four-pole ring-cusp, (c) six-pole line-cusp, and (d) hybrid-cusp. The locations of the antenna are (a)–(d) axial location and (e) radial location. The floating end flange (f) and the bended antenna located close to the ECR zone (g) are also shown.

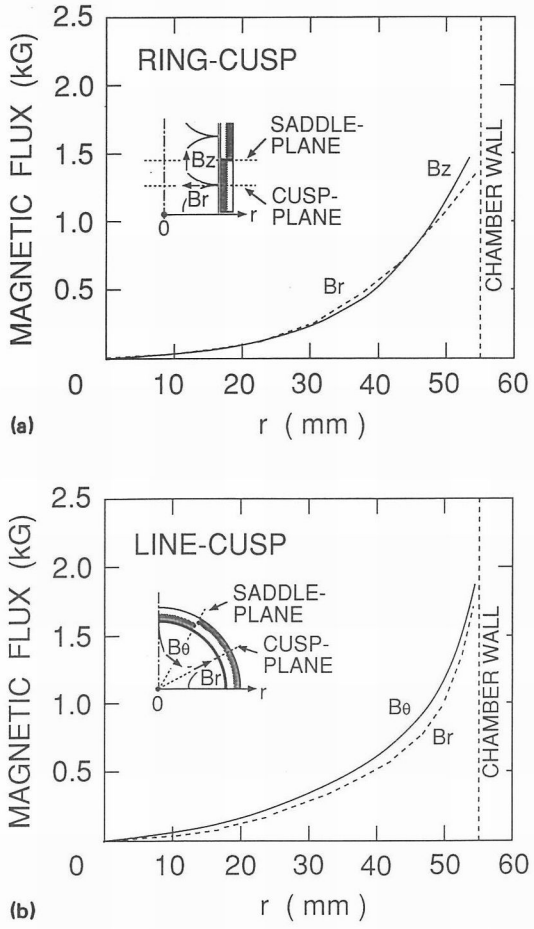

FIG. 2. Magnetic flux density profiles of (a) ring cusp and (b) line cusp. The magnetic field in both saddle and cusp planes are shown.

In this article, attention will be paid mainly to the effect of magnetic configurations and antenna locations on the multicusp ECR discharge. Several simplified cases were compared experimentally and the mechanism of ignition and plasma generation are discussed. In the last part of this article, we also make a short review on the previous works.

II. EXPERIMENT

To study the effect of magnet arrangement, multicusp magnets of seven-pole or four-pole ring-cusp [Figs. 1(a), 1(b), and 1(e)], a six-pole line-cusp [Fig. 1(c)], and a hybrid-cusp [Fig. 1(d)] are prepared. These magnets are constructed by sticking barium ferrite magnets on an 11 cm $\phi \times 30$ cm L stainless-steel cylinder. The separation of each ring-cusp pole is fixed at 4 cm. Figures 2(a) and 2(b) show the profiles of magnetic flux density in a ring-cusp and a line-cusp field. Profiles for both saddle-plane and cusp-plane are shown. The flux density decays rapidly with the distance from the wall surface. The ECR zones of 875 G for 2.45 GHz are located at about 1 cm inside the chamber wall ($r = 45$ mm) in both configurations and both cusp and saddle planes.

A microwave supplied from a 2.45-GHz 5-kW cw magnetron is fed to a coaxial waveguide through an isolator, an *E-H* tuner, a power monitor, and a rectangular to coaxial mode exchanger. The end of the coaxial waveguide is coupled with the discharge chamber. The center electrode of the coaxial waveguide works as a rod antenna of 1 cm $\phi \times 4$ cm L. To study the effect of antenna location, both axial and radial rod antennas are prepared. The axial type antenna shown in Figs. 1(a)–1(d) is located in the weak magnetic field region and may excite a single TM01 waveguide mode. On the other hand, the radial antenna shown in Fig. 1(e) is located in the strong multicusp field region and may excite a single TE11 waveguide mode. The diameter of the discharge chamber is so chosen that the higher waveguide mode is suppressed by the cutoff. Additionally, the length of the chamber is so chosen that the chamber does not work as a microwave resonance cavity. This arrangement allows a simple estimation of microwave field intensity. Two other arrangements of microwave feeding system were also examined to improve the ignition performance of line-cusp device. First, to reduce the edge loss of the line cusp, an electrically floating end flange [Fig. 1(f)] was prepared. Second, to excite a strong rf field near

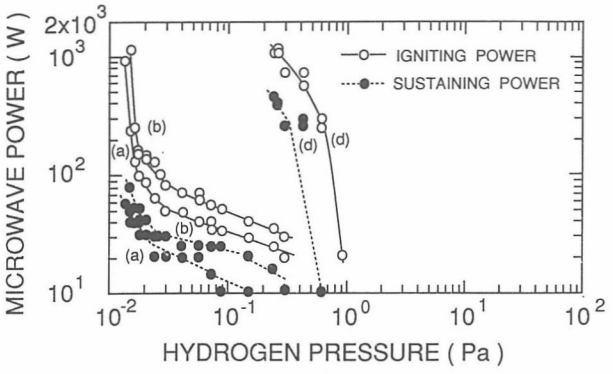

FIG. 3. Igniting and sustaining power as functions of the hydrogen pressure. The results of (a) seven-pole ring cusp, (b) four-pole ring cusp, and (d) hybrid-cusp are shown. Note that the line-cusp device does not give a ignition so that result is not shown here.

the ECR region, a bended rod antenna located close and along with the ECR zone [Fig. 1(g)] was prepared.

The electron density $n_e(\mathrm{cm}^{-3})$, electron temperature T_e (eV), space potential V_s(V), and floating potential V_f(V) were evaluated by cylindrical single Langmuir probes of 1 mm $\phi \times 5$ mm L.[44,45] The spatial distribution of the plasma was measured with sliding or rotating the probe body (see Fig. 1). Plasma parameters at low magnetic field regions were estimated with the electron current component. Because the electron current is suppressed by a transverse magnetic field,[46] the density profiles in strong magnetic fields were studied with ion saturation current I_{is}.

III. RESULTS AND DISCUSSION

A. Effect of magnet arrangements on plasma ignition

Ignitions of a hydrogen plasma in four different multicusp arrangements [Figs. 1(a)–1(d)] were studied with the same microwave feeding system at hydrogen pressures P_{H2} of 10^{-2} Pa to 1 Pa and microwave powers P_{rf} up to 2 kW. Ignition of a simple microwave plasma was also examined removing all magnets form the chamber. The microwave was fed by an axial antenna, which may excite a single TM01 waveguide mode. The length L of the axial antenna was fixed at 4 cm. It is noted that the discharge is not sensitive to the L, when 3 cm $< L <$ 6 cm. This independence on the L can be attributed to the cutoff of the higher waveguide modes.

Igniting powers and sustaining powers as functions of the P_{H2} are shown in Fig. 3. The ring-cusp devices give ignitions at microwave powers as low as 30–100 W and hydrogen pressures as low as 2×10^{-2} Pa. The numbers of the magnet poles make a small difference in the ignition characteristics. The line-cusp devices gives no ignition in the experimental range so that no graph is shown here. The hybrid-cusp device gives ignitions at pressures above 0.1 Pa, however the discharge is not stable. The microwave discharge without magnetic field ignites at higher pressures above 30 Pa, which agrees with the well known microwave discharge in coaxial cylinder.[47] In these experiments, the sustaining power is always smaller than a half of the igniting power.

From these results it is concluded that the ring-cusp device gives a sufficient heating and confinement of electrons to ignite an ECR discharge. The small difference between two different pole numbers of ring cusp, indicates the independent contributions of each (or each pair of) ring-cusp magnet to the ECR discharge. The axial antenna is supposed to excite a single TM01 waveguide mode which has an axial symmetry and the electric field of large radial component near the chamber wall. Then, in the saddle plane of the ring-cusp configuration, electrons are expected to be confined in a local mirror field in the axial direction, and transported in the azimuthal direction due to a drift motion caused by the gradient of the magnetic field (grad-B drift).[48] Because this drift motion keeps its guiding center at the same radial position, the electrons will stay in the ECR zone, efficiently heated by the wave field until a collision changes the electron trajectory. In the cusp plane, electric fields in the radial direction do not contribute to the ECR acceleration and the divergent magnetic field drive electrons out of the ECR zone. These conjectures are confirmed by the light emission observation and probe measurements as described in Sec. III C. Then, if the trajectory of grad-B drift motion is closed or long enough, such as the case of ring-cusp device, the characteristic length Λ for the electron loss is supposed to be comparable to the length of the magnetic line of force because the mirror ratio of the local mirror field is not so large ($B_{\max}/B_{\min} < 2$). Then, the ECR discharge will be ignited when ionization frequency ν_i gets larger than the electron loss frequency along the magnetic field of line. However, because electrons are re-emitted from the chamber wall by secondary electron emission, the effective Λ becomes much longer. If the electron number is sustained without any ionization process in this way, the ECR discharge will be ignited when the ionization rate exceeds the ion loss frequency.

Here, we estimate ECR ignition conditions for a region bounded by walls which absorb electrons and re-emit secondary electrons, on the basis of Brown's theory of high-frequency gas discharge.[49] The continuity equation for electrons is

$$\frac{\partial n_e}{\partial t} = \nu_i n_e + S - \mathrm{div}\Gamma_e, \tag{1}$$

where the term $\nu_i n_e$ is the rate of gain electrons by ionization, S is the rate at which electrons are produced by an external source and normally is very small. In this case, the last term will be expressed as

$$\mathrm{div}\Gamma_e = \alpha n_e \langle v_{e\parallel} \rangle / \Lambda_{\parallel} + \mathrm{div}\Gamma_{e\perp}, \tag{2}$$

where $\langle v_{e\parallel} \rangle$ is the averaged electron velocity component parallel to the magnetic field. The first term describes an electron loss along the magnetic line of force, and the second term that across it. The coefficient α is a new parameter which is introduced to express the electron re-emission effect by secondary electron emission. The α will be unity when the secondary emission rate is negligible, while it will

be very small when secondary emission is frequent. The secondary electron emission process is important because $\nu_i < \langle v_{e\parallel}\rangle/\Lambda_\parallel$ in the pressure range of less than a few Pa.

First, we discuss the case of ring-cusp arrangement, where the last term disappears because $\Gamma_{e\perp}$ is constant at all azimuthal positions. Therefore, the continuity of electrons is expressed as

$$\frac{dn_e}{dt}=\nu_i n_e + S - \alpha n_e \frac{\langle v_{e\parallel}\rangle}{\Lambda_1}. \tag{3}$$

If $\alpha\sim 1$, then $dn_e/dt<0$ and discharge will not start. On the other hand, if the secondary electron emission is frequent and $\alpha\sim 0$, then the last term will be very small and dn_e/dt becomes positive. Assuming some self-limiting effect, such as the space charge effect, the electron density will saturate at a certain value before it reaches a very large value. Because electrons must be accelerated sufficiently by the wave field before it reaches the wall surface, the condition of $\alpha\sim 0$ will define the lower igniting limit of the microwave power. Then, if it is supposed that the electron density is sustained, the ignition is defined by the condition that the ion density goes to infinity. This condition, in turn, will define the lower limit of the discharge pressure. We then consider the following.

An effective secondary electron emission needs incident electron energy of about 100 eV.[50] Considering the energy gain of resonant electrons traveling along the magnetic line of force to the chamber wall, this condition is given by

$$qE_{\rm eff}^2(\Lambda_\parallel/\langle v_{e\parallel}\rangle)^2/2m_e > 100({\rm eV}), \tag{4}$$

where $E_{\rm eff}$ is the effective electric field. Substituting a typical $\langle v_{e\parallel}\rangle$ for a secondary electron (10 eV),[50] we have

$$E_{\rm eff}\Lambda_\parallel > 63({\rm V}). \tag{5}$$

Then, assuming a single TM01 waveguide mode, and using the chamber radius of 5.5 cm and $\Lambda_\parallel = 6$ cm, we have

$$P_{\rm rf} > 120({\rm W}). \tag{6}$$

This value lies in the experimental range obtained at $P_{\rm H2}$ of 2×10^{-2} to 10^{-1} Pa. In detail, the ignition power gradually gets smaller as the pressure increases. It must be due to the increase of the $\nu_i n_e$ term. Next, we estimate the minimum igniting pressure by considering the continuity equation for ions, which is

$$dn_+/dt=\nu_i n_e - {\rm div}\Gamma_+ \tag{7}$$

or

$$dn_+/dt=n_0 n_e\langle\sigma v_e\rangle - n_+ v_+/\Lambda, \tag{7'}$$

where n_0 is the neutral gas density, σ the cross section for ionization, and v_+ the ion thermal velocity. Assuming that $n_e\sim n_+$, ignition occurs when $n_0\langle\sigma v_e\rangle > v_+/\Lambda$. Then using $\sigma = 1\times 10^{-16}$ cm^2, $v_e = 6\times 10^8$ cm/s at 100 eV, and $v_+ = 1.8\times 10^5$ cm/s (H_2^+), we have

$$n_0 > 3.0\times 10^{12}/\Lambda. \tag{8}$$

Substituting the Λ of 1 cm, we have an ignition condition of $n_0 > 3.0\times 10^{12}$ cm^{-3}, which corresponds to 1.1×10^{-2} Pa. This value is close to the lower limit of the igniting pressure of ring-cusp devices.

In the case of line-cusp devices, electrons are driven in the axial direction towards the end flanges by the grad-B drift motion, whose velocity is given by[48]

$$\mathbf{v}_{\rm drift}=(1/2)v_{e\perp}r_L\mathbf{B}\times{\rm grad}B/B^2, \tag{9}$$

where r_L is the electron Larmor radius and $v_{e\perp}$ is the electron velocity perpendicular to the magnetic field. Now, we have gradB/B of about 1 cm^{-1} at the ECR position of the line-cusp device. Then, we have a drift velocity of 1×10^7 cm/s for a 100-eV electron. The effect of this drift motion can be treated by using a modified diffusion length $\Lambda_{\rm eff}$,[51] where the igniting condition is given by

$$\nu_i/D_\perp = 1/\Lambda_{\rm eff}^2, \tag{10}$$

where $\Lambda_{\rm eff}$ is given by the same analysis as the case of superimposed dc electric field,[51] and is defined as

$$1/\Lambda_{\rm eff}^2 = 1/\Lambda^2 + (v_{\rm drift}/2D_\perp)^2. \tag{11}$$

At a hydrogen pressure of 1 Pa and an electron energy of 100 eV, we have $v_{\rm drift}/2D_\perp$ of 10^2 cm^{-1}, $1/\Lambda_{\rm eff}^2$ of 10^4 cm^{-1}, and $\nu_i/D_\perp$ of 5×10^2. Then it follows that $\nu_i/D_\perp \ll 1/\Lambda_{\rm eff}^2$. Therefore the electrons are swept out before ionization and makes it hard to ignite a discharge. The very small value of $\Lambda_{\rm eff}$ emphasize the importance of the continuous cusp field. Accordingly, the line-cusp device using a metal chamber and axial rod antenna does not give an ignition. In this experiment, the hybrid-cusp device, which has a continuous cusp configuration, does not give a stable ignition. It is found that the measured magnetic field at the corner is weaker than that in the line-cusp region. Therefore the div$\Gamma_{e\perp}$ term in Eq. (2) may be large at the corner and reduces the discharge efficiency.

B. Improvement of ignition performance in line-cusp device

We have made some additional experiments to improve the ignition performance of the line-cusp device. First, we changed the grounded end flange of the line-cusp device to be electrically floating as shown in Fig. 1(f). Then the discharge can be ignited at higher microwave power of 700 W. This result indicates the improvement of the electron confinement by the charging of the end flange, where negative charging of the end flange will prevent electrons from sinking into the end flange. Second, we used a bended rod antenna along and very close to an ECR zone of the line-cusp magnet as shown in Fig. 1(g). Then the discharge can be ignited at the microwave power of as low as 25 W and the neutral pressure of 0.13 Pa. In this case, the ignition condition is very sensitive to the antenna position. This result clearly indicates the effect of a strong wave field around the rod antenna.

C. Effect of magnet arrangements on plasma structure

The front view of the light emissions from the ring-cusp plasma [Fig. 1(b)] in the case of 0.03–30 Pa in H_2

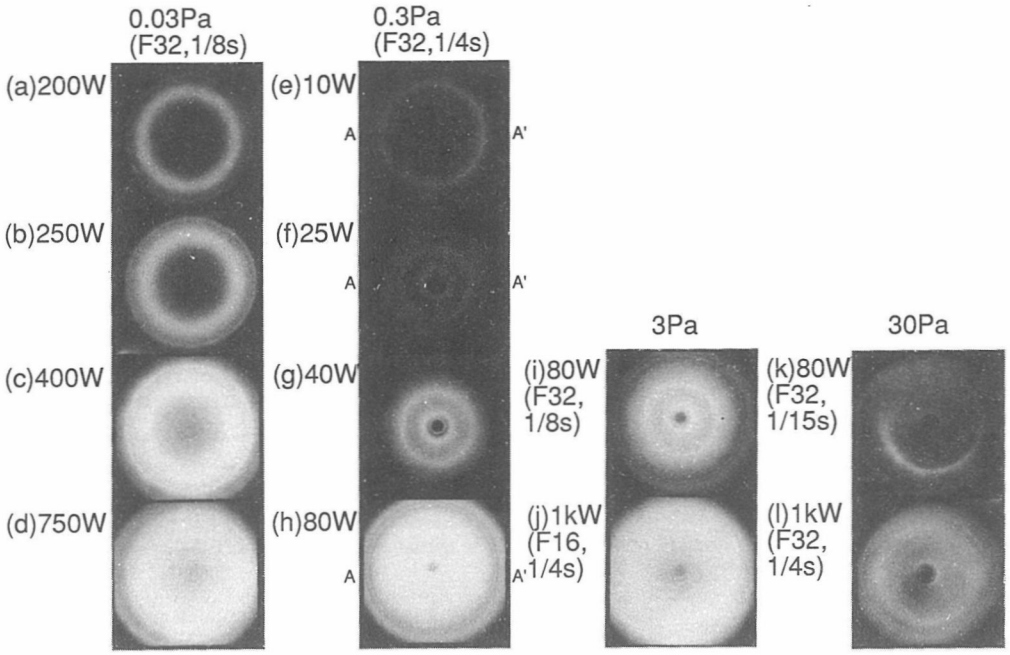

FIG. 4. Light emissions from the ring-cusp plasma. The hydrogen pressure and the microwave power are indicated in the figure. The numbers in the parentheses indicate the F number and the shutter speed of the shots.

pressures and 10 W to 1 kW in microwave powers is shown in Figs. 4(a)–4(l). Figures 5(a), 5(b), and 5(c) are luminosity-meter traces of the photographs for $P_{H2} = 0.3$ Pa. At $P_{H2} = 0.03$ Pa, an annular emission profile near the ECR zone is recognized. It is found from the side view that the luminous region are located between each magnet rows (saddle plane). The emissive region extends inwards as the P_{rf} is increased. At $P_{H2} = 0.3$ Pa and very low P_{rf} of 10 W, a similar profile very close to the ECR zone is recognized [Fig. 5(a)]. Increasing the P_{rf} up to 25 or 40 W [Fig. 5(b)], the light emission profile becomes a shell structure. The emission from the ECR zone gets weak, while that from the higher harmonics resonance region ($\omega \sim 4\omega_c$) and the circumstance of the rod antenna get intense. At $P_{rf} = 80$ W, the emission gets uniform and intense [Fig. 5(c)]. At $P_{H2} = 3$ Pa, the same shell structure is observed. At $P_{H2} = 30$ Pa, the rotative symmetry is broken and a circular arc structure at the ECR zone appears. In these experiments, the light emissions from the ECR zone are recognized in all pressures, while the shell structure is recognized in the moderate pressures. The front view of the light emissions from the hybrid-cusp plasma are shown in Figs. 6(a) and 6(b). At $P_{H2} = 3$ Pa and $P_{rf} = 80$ W [Figs. 6(a)], the emission profile consists of six parts of different brightness, each part of which shows the profile of the local mirror field. At higher pressure of 7 Pa and $P_{rf} = 250$ W [Fig. 6(b)], the emission from the dark sites disappears, and the emission profile becomes a three isolated structure. This discharge mode is not stable and at slightly higher microwave powers, all sites get emissive again.

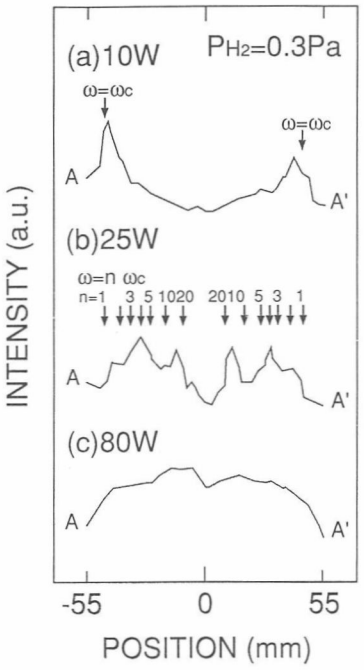

FIG. 5. Luminosity-meter traces of the ring-cusp plasma obtained at hydrogen pressure of 0.3 Pa and microwave powers of 10, 25, and 80 W. Arrows over the curves indicate the ECR conditions.

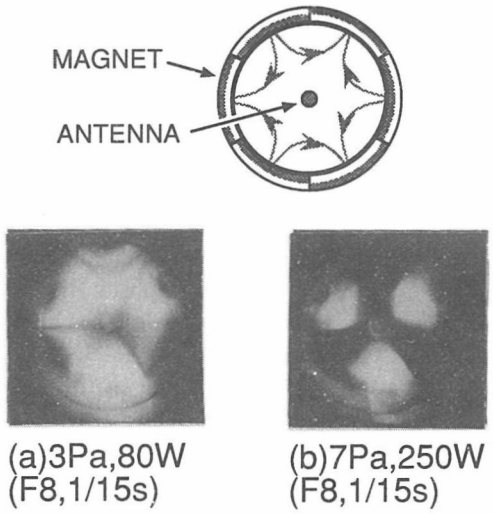

FIG. 6. Light emissions from the hybrid-cusp plasma obtained at (a) 3 Pa, 750 W, (b) 7 Pa, 250 W. The locations of magnets and a rod antenna are shown in the illustration. The numbers in the parentheses indicate the F number and the shutter speed of shots.

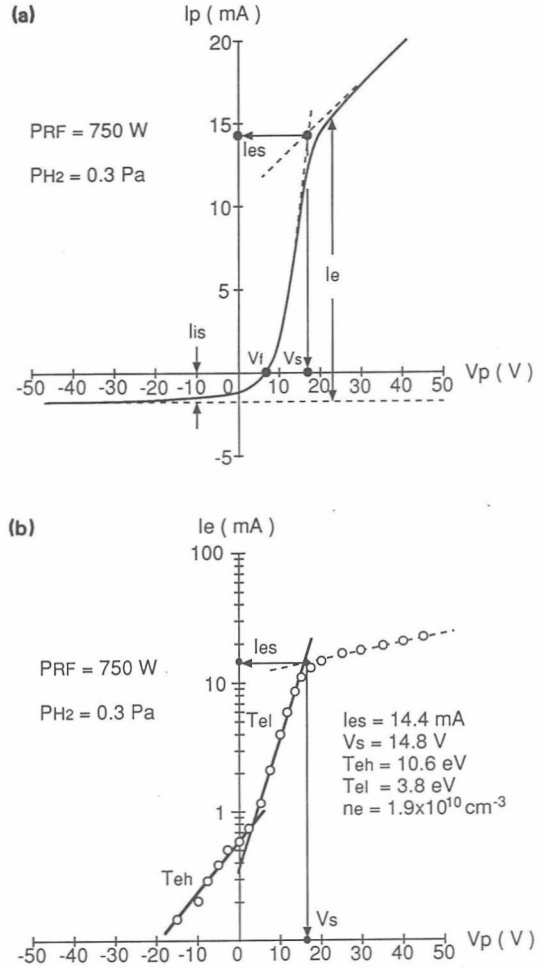

FIG. 7. Typical results of (a) a prove curve and (b) a semi-logarithmic plot of the electron current component (I_e).

This emission profile represents the distribution of the excited species in the plasma. If a mean lifetime of an excited state is short enough, the corresponding light emission profile is not so much different from the excitation profile. The mean lifetime for allowed transition[52] will satisfy this assumption. The profile of excitation will be defined by the location of electron heating and the transport of hot electrons. Then the annular emission from the ECR zone in the saddle plane is the direct evidence of the ECR heating and the electron trap there. In the hybrid cusp, the bright site and the dark site are located in counterclockwise and clockwise magnetic field regions, respectively. Due to the different direction of the magnetic line of force, the electrons in both sites drift to opposite directions. Because the antenna is closer to one side of the chamber than to another side, the resident time of the electron in both sites are different due to the difference in the direction of drift. The bright site is corresponding to the longer residence time.

Next, we consider the inward extension of the emission profile. According to the wave theory in a cold plasma,[53] the angular frequencies of density cutoff, ECR, and upper hybrid resonance (UHR) are given by

$$\omega_p^2 = n_e q^2/\epsilon_0 m_e \quad \text{(cutoff)}, \tag{12}$$

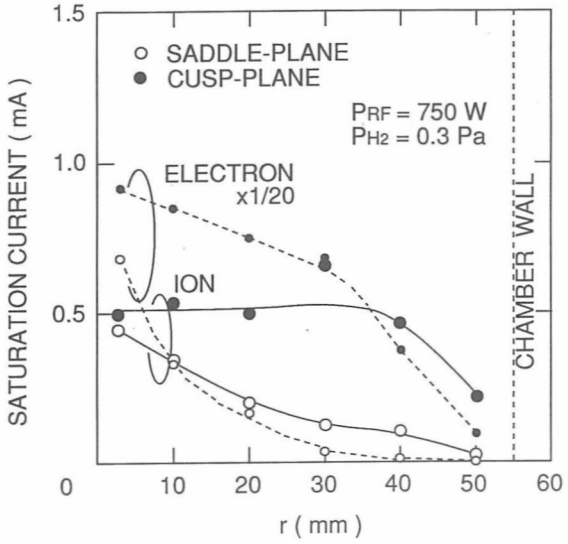

FIG. 8. Radial profiles of ion and electron saturation currents in saddle plane and cusp plane.

$$\omega_c = qB/m_e \quad \text{(ECR)}, \tag{13}$$

$$\omega_{\mathrm{UH}}^2 = \omega_c^2 + \omega_p^2 \quad \text{(UHR)}. \tag{14}$$

Due to the gradient of magnetic field, the UHR zone moves inward as the electron density approaches the cutoff density ($\omega_p = \omega_{\mathrm{rf}}$). In these studies, however, the electron density is expected to be so low ($\omega_p/\omega_c < 0.1$) that the UHR zone is not apart from the ECR zone. The other possible mechanism for the inward extension of the emission profile is the inward transport of hot electrons. Because the diffusion coefficient is larger in the inner position due to the smaller magnetic field, the electron diffusion is directed inward. Additionally, if the electron energy reaches on the order of 10 keV, the electron Larmor radius gets larger than 4 mm at the ECR zone, and the electron passes inner position and excites particles there. The former effect will be dominant at higher pressures and the latter at lower pressures, respectively. The shell structure observed in moderate pressures also indicates the existence of some resonant heating at the bright region of $\omega = 4\omega_c$, while other resonance at $\omega = 2\omega_c$ or $3\omega_c$ was not observed. We now need further study of the detailed structure of the plasma and the microwave field to determine the exact mechanism. On the other hand, the circular arc structure observed at high pressure [Fig. 4(k)] indicates the clockwise motion caused by the gradient-B drift and inward diffusion of electrons. The start point of the arc structure may be related to the incompleteness of the ring-cusp field.

Structure of the ring-cusp plasma is analyzed further by means of the Langmuir probe method. Figures 7(a) and 7(b) show the typical plot of I_p and $\ln(I_e)$. Two components of electron temperatures (T_{eh} and T_{el}) are determined from the slopes in the $\ln(I_e)$ curve. The processes to obtain the values of ion saturation current I_{is}, electron saturation current I_{es}, space potential V_S, and floating potential V_f are shown in the figures. The probe measurements were performed at $P_{\mathrm{H2}} = 0.3$ Pa and $P_{\mathrm{rf}} = 750$ W. The

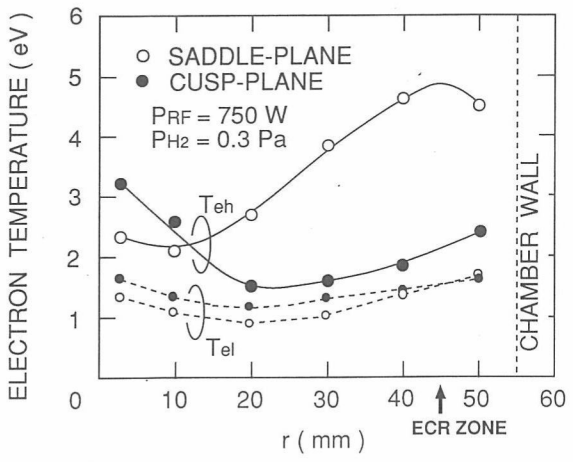

FIG. 9. Radial profiles of electron temperatures (T_{eh} and T_{el}) in saddle plane and cusp plane. The ECR zone is indicated with an arrow.

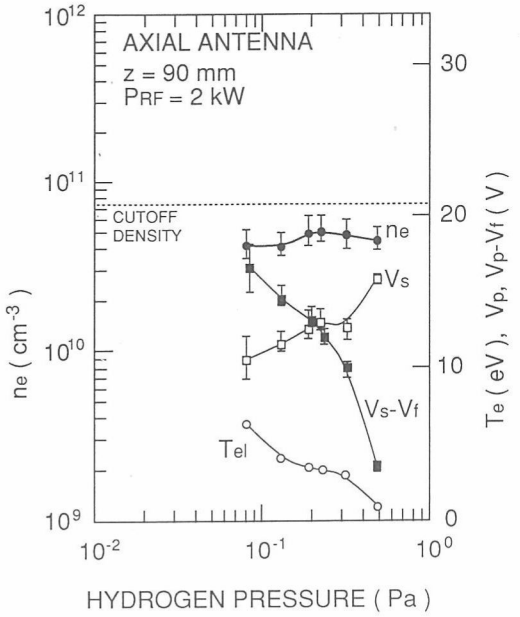

FIG. 10. Plasma parameters vs hydrogen pressure for the axial antenna system at a microwave power of 2 kW.

radial profiles of I_{is} and I_{es} are plotted in Fig. 8. The I_{is} is uniform in the cusp-plane ($z = 117$ mm), and decreases with radial distance in the saddle plane ($z = 137$ mm), indicating the plasma confinement inside the ring-cusp field. On the other hand, the I_{es} decrease with radial distance in both the cusp plane and the saddle plane. The radial variation of the I_{es} is partly due to the static magnetic field. At the center of the cusp plane, the magnetic field is weak and the magnetic line of force is not just along the axis of the cylindrical probe. Accordingly, the I_{es}/I_{is} ratio of about 36 is in the theoretical range of 22–38 corresponding to the effective ion mass number of 1 (H_1^+) to 3 (H_3^+). Figure 9 shows the radial profiles of T_{eh} and T_{el} obtained by the $\ln(I_e)$-V_p plot of the probe data. A clear single peak of T_{eh} is found at the ECR zone of the saddle plane. The two components of electron temperatures (T_{eh} and T_{el}) will correspond to two different groups of electrons. It is considered that T_{eh} and T_{el} correspond to the temperatures for electrons directly heated by the microwave power, and electrons produced by ionizations of neutral hydrogen, respectively. The peak of T_{eh} indicates the efficient plasma heating by ECR process at the ECR zone in the saddle plane. In the center region of the ring-cusp field, abundant plasma may be supplied from the ECR zone by the diffusion[34] or directly produced by the UHR heating or other heating mechanisms such as the stochastic process,[54] so that the excellent confinement by the ring-cusp field will result in a dense plasma generation.

D. Effect of antenna location on plasma generation

To study the effect of antenna location on the plasma generation, both axial and radial antenna location were examined using the four-pole ring-cusp magnet [Figs. 1(b) and 1(e)]. The axial antenna is located in the weak magnetic field region and may excite a single TM01 waveguide mode, while the radial antenna is located in the strong magnetic field region and may excite a single TE11 waveguide mode. Electron densities n_e and electron temperatures T_{eh} and T_{el} were measured by a Langmuir probe fixed at the center of the cusp plane ($r = 0$ mm, $z = 90$ mm) in hydrogen pressures P_{H2} of 0.04–0.5 Pa and microwave powers P_{rf} of 0.5 to 3 kW.

Results for the axial antenna systems are shown in Figs. 10 and 11. Electron densities saturate at the cutoff density[53] of 7.4×10^{10} cm^{-3} in P_{rf} of more than 1 kW. The steep decrease in n_e at lower P_{rf} is due to the change of the impedance matching between the microwave circuit and the plasma. When the impedance matching is carefully carried out, the change of n_e is proportional to the P_{rf} at such lower powers. The electron temperature, which is in the range from 1 to 5 eV, increases weakly as the P_{rf} is increased and decreases as the P_{H2} is increased. Next, results

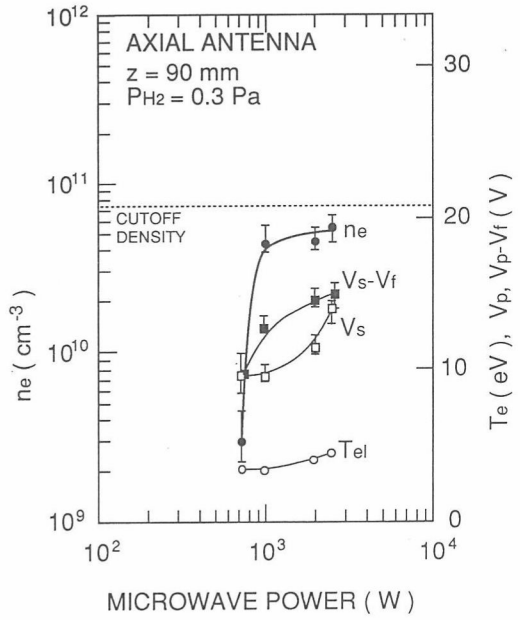

FIG. 11. Plasma parameters vs microwave power for the axial antenna system at a hydrogen pressure of 0.3 Pa.

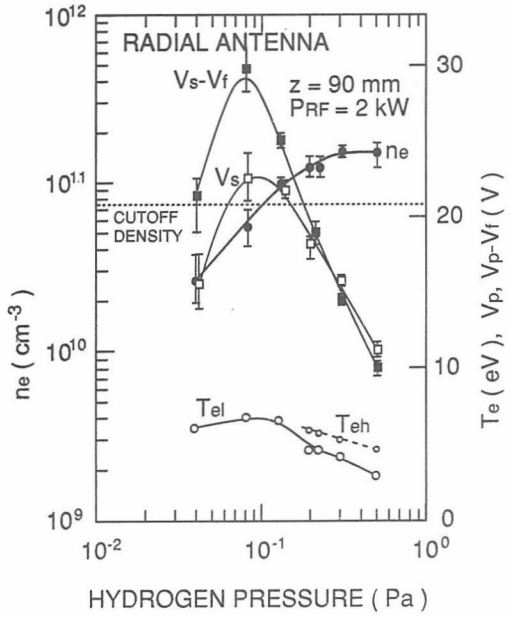

FIG. 12. Plasma parameters vs hydrogen pressure for the radial antenna system at a microwave power of 2 kW.

for the radial antenna system are shown in Figs. 12 and 13. Electron densities proportionally increase with P_{H2} and P_{rf}, and exceed the cutoff density. The electron temperature increases weakly as P_{rf} is increased and has a peak at $P_{H2} = 10^{-1}$ Pa. The electron temperature is 1–2 eV higher than that of the axial antenna system.

The remarkable difference between these two antenna systems appears in the cutoff effect. The axial antenna system shows a clear density saturation, while the radial antenna system shows no cutoff phenomenon. According to the wave theory in a cold plasma,[53] waves propagating in a weak magnetic field region ($\omega_c/\omega \ll 1$) cannot penetrate into a plasma of cutoff density, while a whistler wave propagating in the strong magnetic field region ($\omega_c/\omega > 1$), can propagate along the magnetic line of force at any densities. An extraordinary wave (X wave) which propagates perpendicular to the magnetic line of force can also propagate into the overdense plasma until another cutoff occurs. Therefore, in the case of the axial antenna located in the weak magnetic field region, microwave may be reflected by the plasma of cutoff density, while in the case of the radial antenna located in the strong magnetic field region, microwave can penetrate into the plasma.

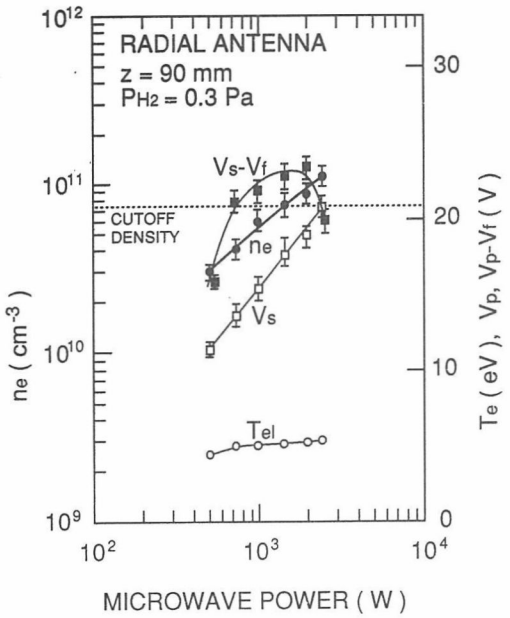

FIG. 13. Plasma parameters vs microwave power for the radial antenna system at a hydrogen pressure of 0.3 Pa.

However, there is a problem in considering the wave propagation in the plasma of this type. The structure of the magnetic field changes in the very short range compared with the wavelength of the plasma waves. For example, the dispersion relation of the whistler wave in an infinite plasma is given by[53]

$$c^2k^2/\omega^2 = 1 - \omega_p^2/\omega^2[1 - (\omega_c/\omega)]. \quad (15)$$

Then due to the large gradient of magnetic field at the ECR zone ($\mathrm{grad}B/B \sim 1$ cm^{-1}), the wavelength becomes smaller than the characteristic length of the multicusp field (4 cm) only within the 10^{-3}-cm-thick region at the ECR zone assuming that $\omega/\omega_p = 10$. This value is not realistic because it is smaller than the Debye length in this plasma ($\sim 10^{-2}$ cm). Almost the same discussion is valid in the case of the X wave. Therefore we cannot analyze the wave propagation in the same manner as in the case of uniform or small gradient magnetic field.[42,43,55] While the mechanism is not clear, these results evidently indicate the importance of a strong magnetic field at the feeding position of the microwave.

E. Discussion

In this article, we have clearly shown the advantage of ring-cusp configuration on the ignition of ECR discharge, and also the effectiveness of the strong magnetic field around the rod antenna on the generation of an overdense plasma. Here, we review the previous works on this point.

Our experiments and considerations on the electron motion have proved the importance to keep the electron trajectory of gradient-B drift motion inside the metal chamber in the ignition of an ECR plasma. It supports the efficient ignition in the ring-cusp device of Neumann and Kretschmer[35] and Goede.[36] Goede compared the electrical efficiency (eV/ion) of azimuthal line cusp (ring cusp) configuration and axial line cusp configuration, while he did not describe the ignition characteristics. He found in his study that the electrical efficiency of the ring-cusp configuration is twice as large as the line-cusp configuration. As is described in his article, however, he could not distinguish the effect of closed drift surfaces from the change of discharge volume which was also by a factor of 2. It is surprising that the electrical efficiency of his line-cusp configuration was not so bad, which is not the case in our study. The difference may come from the larger discharge volume and longer line cusp and the usage of microwave cavity in his device. On the other hand, the devices of

Asmussen and co-workers[25–32] and Pichot and co-workers[33,34] using a line-cusp configuration also ignite successfully. The important point of their approach is that a microwave cavity structure is used in the device of Asmussen, and rod antennas are located close to the ECR zone in the device of Pichot, which enables very high electric field to be exited in the ECR zone. Additionally, electron confinement effect can also be expected by the charge-up on the insulator wall in the case of Asmussen's device, which is also found in our experiment using a floating flange.

Effectiveness of the strong magnetic field in the antenna position on the generation of an overdense plasma is also shown in our experiments. The results agree with the plasma wave theory in an infinite plasma even though the scale length of the magnetic field is very short. This criterion agrees with the result of Pichot *et al.*[33] using rod antennas along the ECR zone and generating an overdense plasma of 10^{11} cm^{-3}. However, Goede observed the density cutoff effect even though the microwave feeding was performed at a strong magnetic region.[36] There seems to be another factor which affects the microwave transport. One of the possibilities is that the extent of the dense plasma into the waveguide reflects the microwave before it reaches the strong magnetic field region. Indeed, an intense plasma glowing inside the coaxial waveguide is observed in our axial antenna configuration device at high power input. In the case of Asmussen's device, an overdense plasma is generated without a multicusp magnet.[25] He explained the mechanism of overdense plasma generation by the penetration of a strong cavity field into the plasma, and its power absorption by a collision process.[56]

On the ECR device using permanent magnets, the effects of the configuration of magnetic fields and the location of feeding antennas have been investigated. First, the importance to keep the electron trajectory of gradient-B drift motion inside the metal chamber is demonstrated in the ignition of an ECR plasma. The ring-cusp magnet gives an efficient ignition due to the good symmetry of the electron trajectory, while the line-cusp magnet hardly gives ignition due to the incompleteness of the electron trajectory. Even in the case of a line-cusp magnet, ignition is achieved by using a floating end flange or a rod antenna very close to the ECR zone. Second, change in the density cutoff effect with different antenna position agrees well with the accessibility of wave field into the resonance point predicted by the plasma wave theory in an infinite magnetized plasma, even though the scale length of the magnetic field is very short.

ACKNOWLEDGMENTS

This work was greatly assisted by the continued efforts of Mr. A. Sugimura, Mr. H. Shiomi, and Mr. J. Kondo. The authors would like to thank Dr. Y. Todokoro, Dr. M. Inoue, and Mr. H. Koide for their continuous encouragement.

[1] B. Lax, W. P. Allis, and S. C. Brown, J. Appl. Phys. **21**, 1297 (1950).
[2] T. Consoli and R. B. Hall, Nucl. Fusion **14**, 93 (1974).
[3] R. Bardet, T. Consoli and R. Geller, Nucl. Fusion **5**, 7 (1965).
[4] R. Geller, IEEE Trans. Nucl. Sci. **23**, 904 (1976).
[5] R. Geller, Appl. Phys. Lett. **16**, 401 (1970).
[6] K. Suzuki, S. Okudaira, N. Sakudo, and I. Kanomata, Jpn, J. Appl. Phys. **16**, 1979 (1977).
[7] M. Matsuoka and K. Ono, Appl. Phys. Lett. **50**, 1864 (1987).
[8] N. Fujiwara, T. Shibano, K. Nishioka, and T. Kato, Jpn. J. Appl. Phys. **28**, 2147 (1989).
[9] J. Ishikawa, Y. Takeiri and T. Takagi, *Proc. International Ion Engineering Congress–ISIAT'83 & IPAT'83, 1983* (IEEJ, Tokyo, 1983), p. 379.
[10] A. Geode, G. J. Brakenhoff, H. J. Hopman, and P. Massmann, Plasma Phys. **15**, 977 (1973).
[11] M. Sadowski, Rev. Sci. Instrum. **40**, 1545 (1969).
[12] R. Limpaecher and K. R. MacKenzie, Rev. Sci. Instrum. **44**, 726 (1973).
[13] K. N. Leung, T. K. Samec, and A. Lamm, Phys. Lett. A **51**, 490 (1975).
[14] K. N. Leung, N. Hershkowitz, and K. R. MacKenzie, Phys. Fluids **19**, 1045 (1976).
[15] A. P. H. Goede and T. S. Green, Phys. Fluids **25**, 1797 (1982).
[16] C. Koch and G. Matthieussent, Phys. Fluids. **26**, 545 (1983).
[17] T. D. Mantei and T. Wicker, Appl. Phys. Lett. **43**, 84 (1983).
[18] J. Pelletier, Y. Arnal, R. Debrie, L. Pomathiod, and J. C. Rifflet, Rev. Sci. Instrum. **55**, 1636 (1984).
[19] T. E. Wicker and T. D. Mantei, Appl. Phys. Lett. **57**, 1636 (1984).
[20] Y. Arnal, J. Pelletier, C. Pomot, B. Petit, and A. Durandet, Appl. Phys. Lett. **45**, 132 (1984).
[21] L. Pomathiod, R. Debrie, Y. Arnal, and J. Pelletier, Phys. Lett. A **106**, 301 (1984).
[22] C. Pomot, B. Mahi, B. Petit, Y. Arnal, and J. Pelletier, J. Vac. Sci. Technol. B **4**, 1 (1986).
[23] J. Pelletier, Y. Arnal, B. Petit, C. Pomot, and M. Pichot, J. Phys. D **19**, 795 (1986).
[24] B. Petit and J. Pelletier, Jpn. J. Appl. Phys. **26**, 825 (1987).
[25] M. Dahimene and J. Asmussen, J. Vac. Sci. Technol. B **4**, 126 (1986).
[26] J. Asmussen and M. Dahimene, J. Vac. Sci. Technol. B **5**, 328 (1987).
[27] J. Hopwood, M. Dahimene, D. K. Reinhard, and J. Asmussen, J. Vac. Sci. Technol. B **6**, 268 (1988).
[28] L. Mahoney, M. Dahimene, and J. Asmussen, Rev. Sci. Instrum. **59**, 448 (1988).
[29] J. Hopwood, D. K. Reinhard, and J. Asmussen, J. Vac. Sci. Technol. B **6**, 1896 (1988).
[30] J. Asmussen, J. Hopwood, and F. C. Sze, Rev. Sci. Instrum. **61**, 250 (1990).
[31] L. Mahoney and J. Asmussen, Rev. Sci. Instrum. **61**, 285 (1990).
[32] J. Hopwood, D. K. Reinhard, and J. Asmussen, J. Vac. Sci. Technol. A **8**, 3103 (1990).
[33] M. Pichot, A. Durandet, J. Pelletier, Y. Arnal, and L. Vallier, Rev. Sci. Instrum. **59**, 1072 (1988).
[34] R. R. Burke and C. Pomot, Solid State Technol. **31**, No. 2, 67 (1988).
[35] G. Neumann and K-H. Kretschmer, J. Vac. Sci. Technol. B **9**, 334 (1991).
[36] H. Goede, J. Spacecr, Rockets **24**, 437 (1987).
[37] O. Fukumasa, A. Nomura, and R. Itatani, *Papers of Technical Meeting on EP-80-23, 1980* (IEEJ, Tokyo, 1980), p. 45 [in Japanese].
[38] R. Itatani and O. Fukumasa, *Proceedings of the 5th Symposium on Ion Sources and Ion-Assisted Technology,* 1981 (IEEJ, Tokyo, 1981), p. 153.
[39] T. Namura, H. Shiomi, A. Sugimura, and R. Itatani, *Papers of Technical Meeting on EP-85-6, 1985* (IEEJ, Tokyo, 1985), p. 45 [in Japanese].
[40] R. Itatani, H. Shiomi, T. Namura, and A. Sugimura, *Proceedings of the 9th Symposium on Ion Sources and Ion-Assisted Technology, 1985* (IEEJ, Tokyo, 1985), p. 59.
[41] R. Itatani, T. Namura, J. Kondo, and H. Murayama, Proceedings of the 10th Symposium Ion Sources and Ion-Assisted Technology, 1986 (IEEJ, Tokyo, 1986), p. 135.
[42] D. G. Swanson, *Plasma Waves* (Academic, New York, 1989), Chap. 5.
[43] D. G. Swanson, *Plasma Waves* (Academic, New York, 1989), Chap. 6.
[44] I. Langmuir and H. Mott-Smith, General Electric Review **27**, 449 (1924).
[45] D. Bohm, *Minimum Ionic Kinetic Energy for a Stable Sheath* (McGraw–Hill, New York, 1949).
[46] J. R. Sanmartin, Phys. Fluids **13**, 103 (1970).

[47] S. C. Brown, *Encyclopedia of Physics vol. 22 Gas Discharges II*, edited by S. Flugge (Springer, Berling, 1956), p. 557.
[48] F. F. Chen, *Introduction to Plasma Physics* (Plenum, New York and London, 1974), Chap. 2, p. 38.
[49] S. C. Brown, *Encyclopedia of Physics Vol. 22 Gas Discharges II*, edited by S. Flugge (Springer, Berlin, 1956), p. 531.
[50] L. N. Tharp and E. J. Scheibner, J. Appl. Phys. **38**, 3320 (1967).
[51] S. C. Brown, *Encyclopedia of Physics Vol. 22 Gas Discharges II*, edited by S. Flugge (Springer, Berlin, 1956), p. 558.
[52] G. Herzberg, *Molecular Spectra and Molecular Structure Vol. 1 Spectra of Diatomic Molecules* (Van Nostrand Reinhold, New York, 1950), 2nd ed., p. 20.
[53] F. F. Chen, *Introduction to Plasma Physics* (Plenum, New York and London, 1974), Chap. 4.
[54] M. A. Lieberman and A. J. Lichtenberg, Plasma Phys. **15**, 125 (1973).
[55] G. Lisitano, M. Fontanesi, and S. Bernabei, Phys. Rev. Lett. **26**, 747 (1971).
[56] J. Root and J. Asmussen, Rev. Sci. Instrum. **56**, 1511 (1985).